SCIENTIFIC REPORTS

OPEN

SUBJECT AREAS:
ELECTROCATALYSIS
ELECTRONIC PROPERTIES AND DEVICES
NANOWIRES
SYNTHESIS AND PROCESSING

Received
13 May 2013

Accepted
22 July 2013

Published
14 August 2013

Correspondence and requests for materials should be addressed to Z.W.C. (zhwchen@uwaterloo.ca)

# Controlled Growth of Platinum Nanowire Arrays on Sulfur Doped Graphene as High Performance Electrocatalyst

Rongyue Wang, Drew C. Higgins, Md Ariful Hoque, DongUn Lee, Fathy Hassan & Zhongwei Chen

Department of Chemical Engineering, Waterloo Institute for Nanotechnology, Waterloo Institute for Sustainable Energy, University of Waterloo, 200 University Avenue West, Waterloo, Ontario, N2L 3G1, Canada.

**Graphene supported Pt nanostructures have great potential to be used as catalysts in electrochemical energy conversion and storage technologies; however the simultaneous control of Pt morphology and dispersion, along with ideally tailoring the physical properties of the catalyst support properties has proven very challenging. Using sulfur doped graphene (SG) as a support material, the heterogeneous dopant atoms could serve as nucleation sites allowing for the preparation of SG supported Pt nanowire arrays with ultra-thin diameters (2–5 nm) and dense surface coverage. Detailed investigation of the preparation technique reveals that the structure of the resulting composite could be readily controlled by fine tuning the Pt nanowire nucleation and growth reaction kinetics and the Pt-support interactions, whereby a mechanistic platinum nanowire array growth model is proposed. Electrochemical characterization demonstrates that the composite materials have 2–3 times higher catalytic activities toward the oxygen reduction and methanol oxidation reaction compared with commercial Pt/C catalyst.**

The synthesis of platinum nanostructures with various morphologies has been extensively investigated over the last decade owing to their widespread applicability in different catalytic reactions such as the oxygen reduction reaction (ORR) and methanol oxidation reaction (MOR) in polymer electrolyte membrane fuel cells (PEMFCs)[1–4]. For fuel cell applications, conventional state-of-the-art catalysts generally consist of Pt and Pt alloy nanoparticles (diameters of 2–5 nm) supported on high surface area, conductive carbonaceous materials in order to facilitate effective mass transport in the catalyst layer and ensure high surface areas and good dispersion of the expensive active materials Despite promising fuel cell performance achieved for this class of catalyst materials, the Pt loading is still too high from an economic standpoint, and durability issues such as Pt dissolution/agglomeration and carbon support corrosion limit the long-term operational stability. These technical challenges can be addressed by the development of improved catalyst support materials[5,6], and by deliberate control of catalyst nanostructures[7,8].

Recently, graphene has been recognized as a promising support for fuel cell catalysts[9,10] owing to its immense surface area (with theoretical specific surface areas as high as ~2600 $m^2 g^{-1}$)[11], high conductivity ($10^3$–$10^4$ S/m)[12], good chemical and electrochemical stability, and availability in bulk amounts[13]. For fuel cell catalyst application, graphene supports are most commonly prepared by subjecting graphene oxide (GO) to a chemical reduction method[9–12]. Inevitably, chemically reduced GO (RGO) still maintain a portion of un-reduced surface functional groups that can serve as nucleation sites for Pt nanoparticle growth; however their conductivity is often much lower than their thermally treated counterparts[10]. Conversely, thermal exfoliation of GO produces relatively defect-free graphene with excellent conductivity; however the deposition of uniformly sized, well dispersed catalyst nanoparticles is very difficult[9,12]. It is thus very challenging to simultaneously control the support functionality along with the catalyst morphology and distribution. Recently, doping graphene with other atoms such as nitrogen[14], or functionalization by a non-covalent approach[15,16] have opened up the possibility of growing catalytically active metals with controllable nanostructures and dispersion on the surface of highly conductive graphene supports.

While appropriate selection of the catalyst support can improve the dispersion and performance of the composite electrocatalyst materials, deliberate control of the deposited Pt nanostructures provides further opportunity to improve the catalytic activity and stability by tuning the arrangement of surface active Pt atoms. Among the different morphologies investigated, nanowires[17–20] or structures consisting of interconnected nanowires such as dendrites[21,22], networks[23], and nanoporous structures[24,25] are particularly sought after because the relative

amount of low-coordinated platinum atoms on their surface is significantly lower than spherical nanoparticles, resulting in higher catalytic activity and durability towards the ORR[25–28]. As most of the methods to make Pt nanostructures with tailored morphologies rely on the delicate control of Pt reduction kinetics and protection of different crystal surface with surfactants, it is not easy to grow these distinct Pt nanostructures directly on the surface of carbon supports[3,4]. To address this, Pt nanostructures are often made separately and then physically mixed with carbon supports which limits catalyst-support "tethering" and may introduce stability issues for fuel cell applications. This highlights the importance of growing Pt nanowires directly on the surface of catalyst supports[29–31], whereby the particular method developed by S. Sun *et al.*[32–35] which uses formic acid as a reducing agent to grow Pt nanowires is very attractive for its simplicity and ease of control.

In this paper, we demonstrate the synthesis of a high density of ultra-thin single crystal Pt nanowire arrays on the surface of sulfur doped graphene (SG) supports using formic acid as a reducing agent at room temperature. SG was selected as this material can be prepared in large quantities by a simplistic high temperature treatment procedure, resulting in sulfur dopant species dispersed homogeneously throughout the entirety of the graphene materials[36]. Despite the possibility to control the composite catalyst functionality by capitalizing on the high affinity between sulfur groups and metal atoms[37], SG has not been previously investigated as a catalyst support. To investigate the growth mechanism in detail, pure graphene (G) was used as a comparison and variations of the synthesis parameters were systematically investigated. Different growth modes of Pt nanostructures on the surface of SG was found in comparison with G, ascribed to the enhanced Pt-support interactions caused by the presence of sulfur groups on the SG surface. This represents for the first time a detailed investigation into the preparation technique of Pt nanowire arrays supported on graphene-based materials, whereby deliberate catalyst nanostructure control can be provided by tailoring the specific catalyst-support surface interactions and offers a new and highly pertinent strategy to synthesize nanocomposite structures with integrated functionality. With favored one-dimensional structures, the electrocatalytic activities of SG supported Pt nanowire arrays (SG-PtNW) towards the ORR and MOR were significantly higher in comparison to commercial Pt/C catalyst which shows great application potential in energy conversion and storage technologies such as PEMFCs.

## Results

The Pt loadings of SG-PtNW samples could be easily controlled by changing the ratio between Pt precursor and SG. Specifically, the Pt loadings of SG-PtNW-1, SG-PtNW-2, SG-PtNW-3 and SG-PtNW-4 samples are calculated to be 66.1, 79.6, 88.6, and 96.5% on the basis of ratio between $H_2PtCl_6$ and SG (see Methods). TGA was conducted on the SG-PtNW-3 sample and the results are shown in Figure S1. Almost no weight loss occurred between room temperature and 300°C, after which obvious weight loss could be observed up until 500°C and ascribed to the oxidation of SG. The residual mass remaining for SG-PtNW-3 (88.5 wt.%) was consistent with the desired platinum loading from the precursor ratios, demonstrating a nearly 100% Pt yield by the formic acid reduction technique. It should be noted that the main weight loss of pure SG was observed between 600 and 750°C, indicating that the presence of Pt catalyzes the combustion of SG at significantly reduced temperatures.

The microstructure of the SG-PtNW-3 sample was characterized using SEM and TEM. As shown in Figure 1 a and b, platinum nanowires with lengths of several tens of nanometers and diameter of several nanometers are seen grown uniformly on the surface of SG. The density of the Pt nanowires is so high that the whole surface of SG was totally covered. Although the orientations of the Pt nanowires are random, these structures can still be considered an array

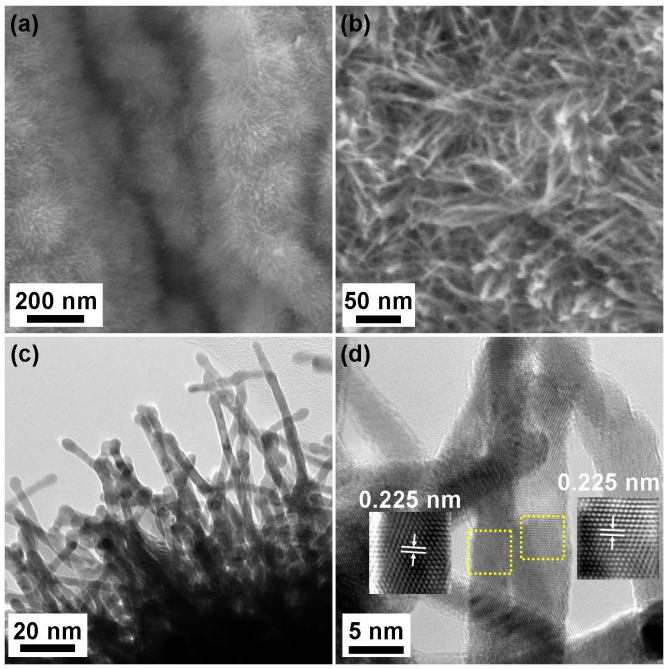


**Figure 1 | (a, b) SEM, (c) TEM and (d) high resolution TEM images of SG-PtNW-3 catalyst.** Insets in (d) are the Fourier filtered high resolution TEM images of the areas highlighted by the dashed yellow squares.

because all of the nanowires project outwards from the support surface. Figure 1 c shows an edge area TEM image of the SG-PtNW-3 sample. From the TEM image it can clearly be seen that the nanowires are grown directly on and perpendicular to the SG surface, possessing relatively uniform diameters of 2–5 nm. From the high resolution TEM images shown in Figure 1 d, it is demonstrated that the Pt nanowires are comprised of single crystals with continuous lattice fringes from the bottom to the top of the nanowires. The Pt nanowires are grown along the <111> direction without exception after examining several nanowires. The observed growth direction is consistent with previously reported results using the polyol process, whereby the formation of single crystal Pt nanowires is associated with the slow growth kinetics of this technique[18]. The lattice spacing between the {111} planes was measured to be 0.225 nm, in direct agreement with that of bulk Pt. The face-centered cubic (FCC) structure of the Pt nanowires was also confirmed by the XRD pattern shown in Figure S2.

Interestingly it was observed that the resulting structures of the SG-PtNW catalysts were highly dependent on the Pt loadings used during preparation. At a lower Pt loading of 66.1 wt.% (SG-PtNW-1), only short Pt nanowires were grown on the surface of SG (Figure 2a and Figure S3), albeit with good distribution indicating the uniform nucleation of Pt (see Figure 2a). Longer Pt nanowires could be obtained by increasing the Pt loading to 79.6 wt.% (SG-PtNW-2, Figure 2b), with even longer lengths observed at a loading of 88.6% (SG-PtNW-3, Figure 2c). A further increase in the Pt loading to 96.5 wt.% (SG-PtNW-4) however resulted in large Pt aggregates formed in the presence of the Pt nanowire arrays (Figure 2d). The coverage of the entire SG surface by short Pt nanowires, along with the absence of any long nanowires on the low Pt loading sample (SG-PtNW-1) indicates that the Pt nanowire growth begins only when the Pt nucleation has occurred on the whole surface of SG. These results demonstrate that the nucleation of Pt on the vacant surface anchoring sites of SG is favorable in comparison to subsequent Pt nanowire growth. Contrastingly, a previous investigation using carbon black supports found that Pt nanowires could be formed at Pt loadings as low as 10 wt.%[34], illustrating the important

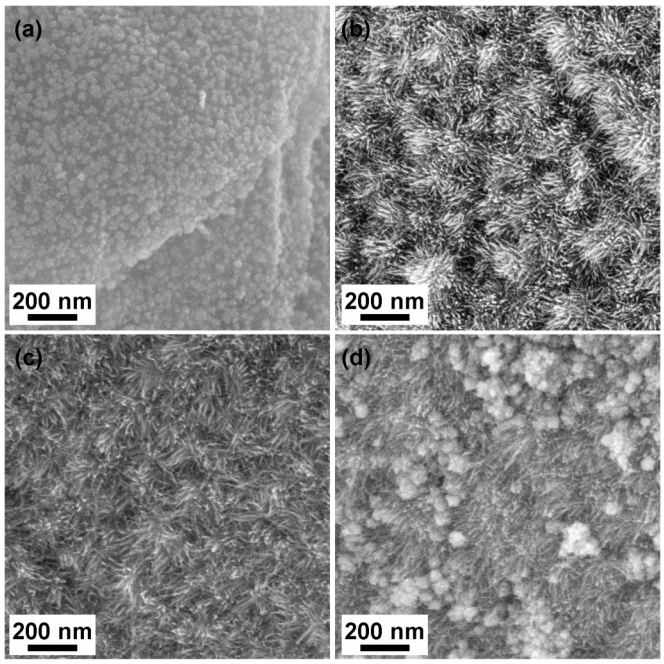


**Figure 2** | **SEM images of (a) SG-PtNW-1, (b) SG-PtNW-2, (c) SG-PtNW-3 and (d) SG-PtNW-4.**

impact of the catalyst support properties and surface species on the Pt nanowire deposition and growth technique. On the other hand, it is well known that the rate of Pt nucleation is controlled by the concentration of zero-valent metal atoms in the growth solution, which is determined directly by the competition between the formation and consumption kinetics[3]. When the growth induced consumption of the metal atoms lags behind their formation, new nuclei are continuously formed regardless of the difference of support materials. Thus the reactant concentrations should also be investigated in order to modulate the rates of nucleation and to fully understand the underlying growth mechanism.

To properly investigate the SG supported Pt nanowire preparation technique, we investigate both the effect of the support materials utilized and of the reactant concentrations/reaction kinetics on the process. For the latter, although it is not possible to control the Pt nucleation and subsequent nanowire growth processes separately, we can decrease the nucleation rate by using lower precursor concentrations.

Figure 3 a and a' show SEM images of G-PtNW-1 with a Pt loading of 66.1 wt.%. It is surprising that even on un-doped G, Pt nucleation is very uniform over the entirety of the support surface, similar with that of SG. Moreover, as shown in Figure S 4a and a', long Pt nanowires together with some Pt aggregates could be grown on G by increasing the Pt loading to 95 wt.% (G-PtNW-4), which is also similar with that of SG. Therefore, under these growth conditions it appears that the differences between the G and SG supports have a minimal effect on the Pt nucleation and subsequent nanowire growth. This might be caused by the fast nucleation process at relatively high reactant concentrations.

Figure 3b and b' show the SEM images of the G-PtNW sample with a Pt loading of 66.1 wt.% prepared under the same conditions except for the concentrations of G and the Pt precursor are half of the typical synthesis condition. It is obvious that the Pt nanowires are much longer, however present in much lower density in comparison to the G-PtNW-1 sample prepared at higher reactant concentrations (Figure 3a and a'). Both of these observations reveal that at reduced precursor concentrations, nanowire growth becomes more favorable than the formation of new nuclei, similar with previous results reported for carbon black supports[34]. The same trends could also be seen on 95% (Figure S4b and b') and 50.6% (Figure S5a and a') Pt loading samples. These results demonstrate that the nucleation of Pt on G can be inhibited when lower Pt reactant concentrations are utilized, whereas the growth process of nanowire structures was not affected greatly. In contrast to the non-uniform growth of Pt nanowires on G in dilute solutions, very uniform Pt nanowire arrays could still be grown on SG under the same dilute conditions (Figure 3c, c' and Figure S4c, c'). From these results, it appears that the primary difference between the two support materials is the higher density of anchoring sites on SG in comparison to G that remain favorable for Pt nucleation under lower reactant concentrations. This is most likely caused by the strong metal-support interactions between SG and Pt. To further support our hypothesis, we investigated the sulfur distribution on the SG sample using EDS elemental quantitative analysis and mapping. The overall EDS spectrum is provided in

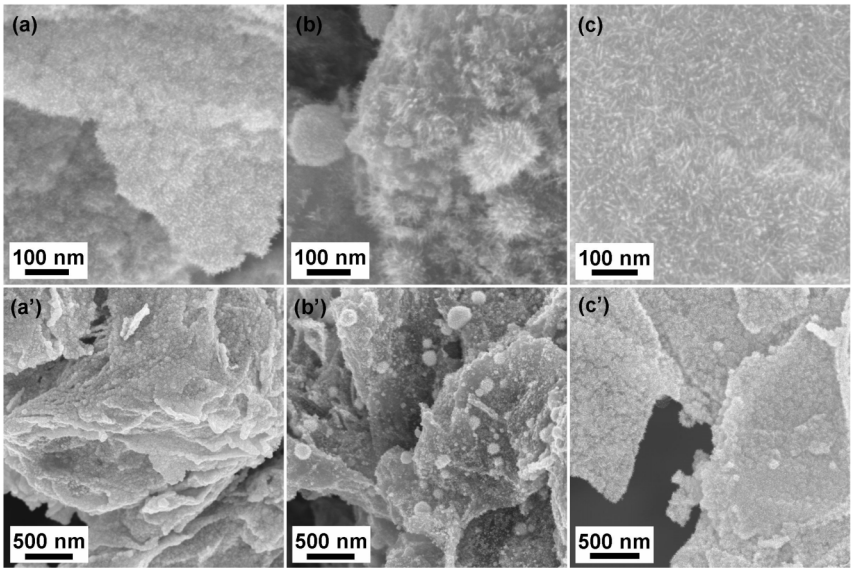


**Figure 3** | **SEM images of Pt nanowires grown on G or SG with Pt mass loading of 66.1%.** Sample in a and a' was synthesized using G as support under the typical synthesis conditions. Sample in b, b' and c, c' were synthesized using G and SG as support, respectively; with both the concentrations of graphene materials and Pt precursor are half of the typical synthesis conditions.

Figure S6, whereby the overall sulfur content is ca. 2.1 at.% which is similar with reported results using a similar sulfur precursor[36]. As shown in Figure S7, the sulfur distribution is quite uniformly distributed both on the graphene sheets and outer edges.

## Discussion

It is well known that sulfur species have strong binding energy with Pt surfaces, commonly causing implications in terms of surface poisoning for catalytic application[37]. This strong SG-Pt interaction offers reasonable explanation for the propensity of Pt ions to form new nucleation sites as opposed to nanowire growth at lower Pt loadings. In fact, only uniformly distributed Pt nanoparticles were observed on SG when the Pt loading is lower than 50%, while Pt nanowire growth on G has already begun at similar Pt loading (Figure S5a and a') . These sulfur sites were believed to interact with Pt atoms and facilitate the initial nucleation despite the precursor concentration. Comparing the results of SG-PtNW-3 and the catalyst materials prepared using identical platinum loadings but lower reactant concentrations, it is observed that the only difference in terms of catalyst nanostructure is that the density of Pt nanowire formation is slightly higher under the dilute conditions. The increased nucleation density on SG in dilute solution is most likely caused by the competition between nucleation and growth which is still not clear and needs further investigation.

The preparation process and proposed growth mechanism of G and SG supported Pt nanowires is summarized in Figure 4, highlighting the impact of support type and Pt loading/concentration. In general, the Pt nanowires grow longer with an increase in Pt loading, although non-uniform aggregates form when the loading is too high. Sulfur doping of graphene increases the metal-support interactions and facilitates favorable nucleus formation, although the difference between SG and G supported Pt nanowires could not be distinguished when grown with high precursor concentrations, most likely due to the rapid kinetics of Pt nucleation.

As mentioned previously, nanowire structures are desirable in terms of ORR activity due to the lower percentage of low-coordinated surface atoms in comparison with Pt nanoparticles. Compared with high-coordinated terrace Pt atoms the low-coordinated surface atoms have higher binding energies with oxygenated species that are believed to be active site blocking species[39]. In addition to the nanowire structure, high temperature derived graphene supports can provide excellent conductivity that ensures the rapid transport of electrons to the catalytically active sites, a very important consideration for electrocatalysis applications such as PEMFC technologies[10]. We have investigated the electrochemical properties of SG-PtNW-3 catalyst, along with its electrocatalytic activity towards the ORR and MOR, two important electrochemical reactions. CV curves of SG-PtNW-3 are shown in Figure 5a, along with commercial Pt/C catalyst

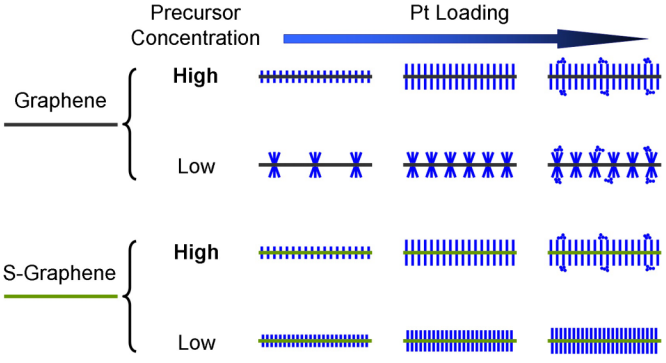


**Figure 4 | Schematic illustration of the nanostructural evolution of Pt nanowire arrays grown on G and SG supports with different precursor concentrations as a function of Pt loading.**

for comparison. The different shapes of the hydrogen under-potential adsorption and de-sorption (H-UPD) peaks observed between 0.06 and 0.36 V reveal the different Pt crystal exposure between the two catalysts. Compared with Pt/C, SG-PtNW-3 shows a sharp Pt oxide reduction peak at a higher potential (0.76 versus 0.73 V), revealing a weakening of the bond between oxygen containing species and the Pt surface, a property linked to increased ORR performance[39]. By determining the charge transfer for hydrogen adsorption/desorption, the electrochemical active surface area (ECSA) could be determined assuming a charge transfer of 210 $\mu C\ cm^{-2}$ Pt surface[5,27]. Based on the Pt loading on the electrode, the ECSA of Pt/C and SG-PtNW-3 were found to be 53 and 40 $m^2\ g_{Pt}^{-1}$, respectively, indicating that the utilization of SG-PtNW-3 is approaching that of commercial Pt/C catalyst.

The ORR activities of Pt/C and SG-PtNW-3 were investigated in $O_2$-saturated 0.1 M $HClO_4$ solution at 30°C, with the results shown in Figure 5b–e. As shown in Figure 5b, the geometric area specific ORR polarization curves exhibit the characteristic profile of two different potential regions, the first, a mixed kinetic/diffusion controlled region above 0.8 V, and the second, a well defined diffusion controlled region below 0.8 V. Although the ECSA of SG-PtNW-3 sample is a little lower than Pt/C catalyst, it exhibits a much higher half-wave potential (0.885 versus 0.866 V), indicating a significant enhancement in the ORR activity. Figure 5c show the ORR polarization curves obtained for SG-PtNW-3 at different rotation speeds, and the corresponding Koutecky-Levich (K-L) plot (Figure 5d) was derived from the K-L equation (1):

$$\frac{1}{j} = \frac{1}{j_k} + \frac{1}{B\omega^{1/2}} \tag{1}$$

where j is measured current density, $j_k$ is kinetic current density, ω is rotation speed, B is a constant. From equation (1) and Figure 5d the constant B was experimentally measured to be 0.096 $mA/s^{1/2}$. The constant B could be also calculated using equation (2):

$$B = 0.62nFAD_{O_2}^{2/3}\ v^{-1/6}C_{o_2} \tag{2}$$

where F is Faraday constant, A is electrode geometry area, $D_{O2}$ is the experimental measured diffusion coefficient of $O_2$ ($1.93 \times 10^{-5}\ cm^2\ s^{-1}$), ν is kinetic viscosity of the solution ($1.009 \times 10^{-2}\ cm^2\ s^{-1}$), and $C_{O2}$ is the concentration of dissolved O2 in solution ($1.26 \times 10^{-3}\ mol\ L^{-1}$)[26]. The excellent agreement of the experimentally measured value of B (0.096 $mA/s^{1/2}$) with the calculated value by assuming n = 4 (0.092 $mA/s^{1/2}$) indicates the dominant 4 electron reduction process of ORR on SG-PtNW-3 catalyst. The ECSA specific kinetic current densities as a function of potential are shown in Figure 5e. It is obvious that the kinetic current densities of SG-PtNW-3 are higher than that of Pt/C throughout the entire potential range investigated (for example 2 times higher at 0.9 V vs. RHE), highlighted the improved ORR kinetics on highly coordinated Pt atoms existent on the surface of the nanowire arrays. We moreover believe the performance could be improved further if the residual low-coordinated Pt atoms were removed using post treatment procedures[26].

In addition to the ORR at the cathode of PEMFCs, the MOR occurring at the anode is also of significant importance as it is critical to the performance of direct methanol fuel cells which hold great potential for small portable device applications[40]. The electrocatalytic activity of SG-PtNW-3 sample was measured in 0.1 M $HClO_4$ + 0.5 M $CH_3OH$ solution and the results are shown in Figure 5f with Pt/C as comparison. SG-PtNW-3 showed higher current densities for both the forward and backward scans which indicate significantly enhanced catalytic activity compared with Pt/C catalyst. Specifically, the ECSA specific current density enhancement for SG-PtNW-3 at a potential of 0.87 V vs. RHE is 3.2 times that of Pt/C (1.6 and 0.5 mA $cm^{-2}$, respectively), meaning that on average, every electrochemically active Pt surface atom on SG-PtNW-3 can catalyze 3 times more

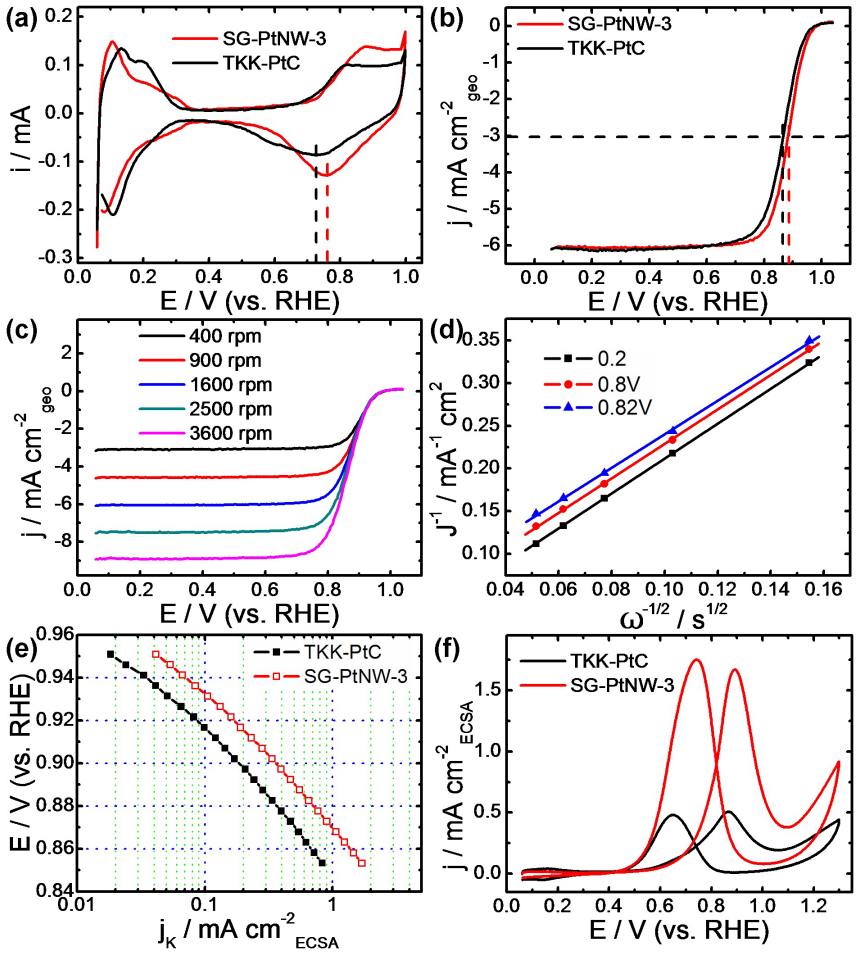


**Figure 5 | Electrochemical and electrocatalytic results of SG-PtNW-3 and commercial Pt/C catalysts.** (a) CV curves of Pt/C and SG-PtNW-3 in 0.1 M $HClO_4$ solution saturated by $N_2$ at a scan rate of 50 mV $s^{-1}$. (b) Forward CV curves for SG-PtNW-3 and Pt/C catalysts in 0.1 M $HClO_4$ solution saturated with $O_2$ at a scan rate of 10 mV $s^{-1}$ and electrode rotation speed of 1600 rpm. (c) ORR polarization curves and (d) Koutecky-Levich plots of SG-PtNW-3 at electrode rotation speeds of 400, 900, 1600, 2500 and 3600 rpm under the same conditions as (b). (e) Specific kinetic current densities ($j_k$) of SG-PtNW-3 and Pt/C catalysts for ORR at different potentials. (f) Specific current densities of SG-PtNW-3 and Pt/C catalysts with the function of potentials toward MOR in 0.1 M $HClO_4$ + 0.5 M $CH_3OH$ mixed solution at a scan rate of 50 mV $s^{-1}$.

methanol molecules than Pt/C within the same period of time. It is worthwhile to note that numerous researchers use the current density peak ratio between the forward scan and the backward scan as an indicator of poisoning resistance. However, recently it has been reported that this method is not suitable for measuring the poisoning resistance of catalyst materials because the current observed in both the forward and backward scan share the same chemical origin[41], and this analysis will not be provided herein.

In conclusion, SG supported ultra-thin Pt nanowire arrays have been successfully synthesized by a formic acid preparation technique. The detailed reaction parameters for catalyst synthesis have been investigated to provide insight into the nanostructure formation mechanism. It was found that when using high concentration precursor solutions, the fast reduction of Pt ions could ensure uniform nucleation on both sulfur-doped and pristine graphene surfaces. This was subsequently followed by the growth of nanowire structures provided that the Pt loading is high enough. Conversely, in low concentration precursor solutions, the strong Pt-S interaction is essential in contributing to the uniform nucleation of Pt on SG, whereas non-uniform nucleation was observed on pristine graphene supports. Based on the rigorous investigations of the Pt nanowire arrays grown on graphene-based support preparation technique, a specific growth model is proposed. Moreover, effectively coupling Pt nanowire structures with high surface area and conductive support materials, the Pt nanowire arrays grown on SG showed significantly enhanced catalytic activity towards both the ORR and MOR in comparison with state-of-the-art Pt/C catalyst. These results effectively demonstrate the great application potential of these catalyst materials for PEMFC applications, and furthermore, the detailed investigation of catalyst preparation and the growth model proposed can provide valuable insight towards the synthesis of new composite electrocatalyst nanostructures.

## Methods

**Preparation of G and SG.** GO was made from natural graphite flakes by the modified Hummer method[38]. To prepare SG, phenyl disulfide (PDS) and GO with a mass ratio of 1 : 1 were mixed together in ethanol by ultrasonication for at least 30 min. After evaporating ethanol, the solid was transferred into a quartz tube and heated in a furnace at 1000°C for 30 min under the protection of high purity Argon[36]. Pure G was made from GO under the same conditions without adding PDS.

**Preparation of SG-Pt and G-Pt.** To grow Pt nanowire arrays on the support materials, G or SG was first dispersed in ultra-pure water by ultrasonication for at least 1 h to make a suspension with a concentration of 1 mg $ml^{-1}$. Then, 2 ml of 20 mM $H_2PtCl_6 \cdot 6H_2O$ solution was mixed together with the proper amount of this suspension in a reactor vessel, and the total solution volume was adjusted to 13.32 ml with ultra-pure water. After thorough mixing, 0.68 ml of formic acid was added to the suspension and left undisturbed at room temperature (ca. 22°C) for more than 3 days. Finally the catalyst was washed with ultra-pure water and ethanol several times and dried at 60°C in an oven overnight. The Pt loading was controlled by adjusting the amount of G or SG solution added without changing any other parameters. Pt mass

loadings of 66.1, 79.6, 88.6, and 96.5% were achieved by using 4, 2, 1, and 0.4 ml of the G or SG solutions, and the products are denoted as SG-PtNW-1, SG-PtNW-2, SG-PtNW-3, and SG-PtNW-4, respectively. In order to investigate the growth mechanism by varying the reaction kinetics, the concentration of both the support and the Pt precursor in the reactor vessel was controlled to be half of the typical synthesis conditions without changing other parameters.

**Material characterization.** The catalyst was adhered to conductive carbon tape directly for scanning electron microscopy (SEM) characterization using a Zeiss ULTRA plus field emission SEM with a working distance of 10 cm. For energy dispersive x-ray spectroscopy (EDS) mapping the sample was loaded on aluminum foil to eliminate signal interference from the carbon tape. For transmission electron microscopy (TEM) imaging the catalyst was dispersed in methanol and loaded onto a copper grid for characterization using a JEOL 2010F TEM at 200 kV. X-ray diffraction (XRD) patterns were collected on an Inel XRG 3000 diffractometer using monochromatic Cu Kα x-rays (0.154 nm wavelength). Thermogravimetric analysis (TGA) was conducted using a Q500 V20.13 TA instrument with a heating rate of 10°C $min^{-1}$ in air.

**Electrochemical characterization.** To prepare the electrode for electrochemical testing, the catalyst materials were first dispersed in 2 ml of ethanol containing 5 μl (15 wt.%) Nafion solution by sonication for at least 30 min and then loaded onto the glassy carbon electrode with a diameter of 5 mm. The loading of commercial Pt/C and SG-PtNW-3 catalysts were controlled to be 20 and 23.6 $\mu g_{Pt}\ cm^{-2}$, respectively. For the SG-PtNW-3 sample, 20% weight percent of carbon black was added to the suspension to increase the dispersion of catalyst on the electrode. After drying in air, the electrode was washed thoroughly using ultra-pure water and mounted on the rotating electrode system. The 0.1 M $HClO_4$ electrolyte solution was purged with high purity $N_2$ for at least 30 min to remove any dissolved oxygen. Cyclic voltammetry (CV) between 0.06 and 1.3 V vs. RHE at a scan rate of 50 mV $s^{-1}$ was performed to activate the catalyst surface until a steady-state CV curve was established. ORR polarization curves were obtained by CV cycling between 0.06 and 1.05 V at a scan rate of 10 mV $s^{-1}$ in oxygen saturated 0.1 M $HClO_4$ and the positive scan was used for ORR performance evaluation. For MOR, the activities were monitored using CV between 0.06 and 1.3 V in a 0.1 M $HClO_4$ + 0.5 M $CH_3OH$ electrolyte mixture at a scan rate of 50 mV $s^{-1}$. The internal resistance (IR) drop was compensated before the CV experiment to reduce the possible resistance in solution.


1. Yu, W. T., Porosoff, M. D. & Chen, J. G. G. Review of Pt-Based Bimetallic Catalysis: From Model Surfaces to Supported Catalysts. *Chem. Rev.* **112**, 5780–5817 (2012).
2. Chen, A. C. & Holt-Hindle, P. Platinum-Based Nanostructured Materials: Synthesis, Properties, and Applications. *Chem. Rev.* **110**, 3767–3804 (2010).
3. Xia, Y. N., Xiong, Y. J., Lim, B. & Skrabalak, S. E. Shape-Controlled Synthesis of Metal Nanocrystals: Simple Chemistry Meets Complex Physics? *Angew. Chem. Int. Ed.* **48**, 60–103 (2009).
4. You, H. J., Yang, S. C., Ding, B. J. & Yang, H. Synthesis of colloidal metal and metal alloy nanoparticles for electrochemical energy applications. *Chem. Soc. Rev.* **42**, 2880–2904 (2013).
5. Higgins, D. C., Meza, D. & Chen, Z. W. Nitrogen-Doped Carbon Nanotubes as Platinum Catalyst Supports for Oxygen Reduction Reaction in Proton Exchange Membrane Fuel Cells. *J. Phys. Chem. C* **114**, 21982–21988 (2010).
6. Higgins, D. C., Choi, J. Y., Wu, J., Lopez, A. & Chen, Z. W. Titanium nitride-carbon nanotube core-shell composites as effective electrocatalyst supports for low temperature fuel cells. *J. Mater. Chem.* **22**, 3727–3732 (2012).
7. Chen, Z. W., Waje, M., Li, W. Z. & Yan, Y. S. Supportless Pt and PtPd nanotubes as electrocatalysts for oxygen-reduction reactions. *Angew. Chem. Int. Ed.* **46**, 4060–4063 (2007).
8. Higgins, D. C., Ye, S. Y., Knights, S. & Chen, Z. W. Highly Durable Platinum-Cobalt Nanowires by Microwave Irradiation as Oxygen Reduction Catalyst for PEM Fuel Cell. *Electrochem. Solid-State Lett.* **15**, B83–B85 (2012).
9. Yoo, E. *et al.* Enhanced Electrocatalytic Activity of Pt Subnanoclusters on Graphene Nanosheet Surface. *Nano Lett.* **9**, 2255–2259 (2009).
10. Kauffman, D. R. & Star, A. Graphene versus carbon nanotubes for chemical sensor and fuel cell applications. *Analyst* **135**, 2790–2797 (2010).
11. Huang, C. C., Li, C. & Shi, G. Q. Graphene based catalysts. *Energy Environ. Sci.* **5**, 8848–8868 (2012).
12. Guo, S. J., Dong, S. J. & Wang, E. K. Three-Dimensional Pt-on-Pd Bimetallic Nanodendrites Supported on Graphene Nanosheet: Facile Synthesis and Used as an Advanced Nanoelectrocatalyst for Methanol Oxidation. *Acs Nano* **4**, 547–555 (2010).
13. Segal, M. Selling graphene by the ton. *Nature Nanotechnol.* **4**, 611–613 (2009).
14. Zhou, Y. K. *et al.* Enhancement of Pt and Pt-alloy fuel cell catalyst activity and durability via nitrogen-modified carbon supports. *Energy Environ. Sci.* **3**, 1437–1446 (2010).
15. Georgakilas, V. *et al.* Functionalization of Graphene: Covalent and Non-Covalent Approaches, Derivatives and Applications. *Chem. Rev.* **112**, 6156–6214 (2012).
16. Ding, M. N., Tang, Y. F. & Star, A. Understanding Interfaces in Metal-Graphitic Hybrid Nanostructures. *J. Phys. Chem. Lett.* **4**, 147–160 (2013).
17. Cademartiri, L. & Ozin, G. A. Ultrathin Nanowires - A Materials Chemistry Perspective. *Adv. Mater.* **21**, 1013–1020 (2009).
18. Chen, J. Y., Herricks, T., Geissler, M. & Xia, Y. N. Single-crystal nanowires of platinum can be synthesized by controlling the reaction rate of a polyol process. *J. Am. Chem. Soc.* **126**, 10854–10855 (2004).
19. Wang, C., Hou, Y. L., Kim, J. M. & Sun, S. H. A general strategy for synthesizing FePt nanowires and nanorods. *Angew. Chem. Int. Ed.* **46**, 6333–6335 (2007).
20. Guo, S. J., Zhang, S., Sun, X. L. & Sun, S. H. Synthesis of Ultrathin FePtPd Nanowires and Their Use as Catalysts for Methanol Oxidation Reaction. *J. Am. Chem. Soc.* **133**, 15354–15357 (2011).
21. Lim, B. & Xia, Y. N. Metal Nanocrystals with Highly Branched Morphologies. *Angew. Chem. Int. Ed.* **50**, 76–85 (2011).
22. Peng, Z. M. & Yang, H. Synthesis and Oxygen Reduction Electrocatalytic Property of Pt-on-Pd Bimetallic Heteronanostructures. *J. Am. Chem. Soc.* **131**, 7542–7543 (2009).
23. Song, Y. *et al.* Synthesis of platinum nanowire networks using a soft template. *Nano Lett.* **7**, 3650–3655 (2007).
24. Wang, R. Y., Xu, C. X., Bi, X. X. & Ding, Y. Nanoporous surface alloys as highly active and durable oxygen reduction reaction electrocatalysts. *Energy Environ. Sci.* **5**, 5281–5286 (2012).
25. Kibsgaard, J., Gorlin, Y., Chen, Z. B. & Jaramillo, T. F. Meso-Structured Platinum Thin Films: Active and Stable Electrocatalysts for the Oxygen Reduction Reaction. *J. Am. Chem. Soc.* **134**, 7758–7765 (2012).
26. Koenigsmann, C., Zhou, W. P., Adzic, R. R., Sutter, E. & Wong, S. S. Size-Dependent Enhancement of Electrocatalytic Performance in Relatively Defect-Free, Processed Ultrathin Platinum Nanowires. *Nano Lett.* **10**, 2806–2811 (2010).
27. Sun, S. H. *et al.* A Highly Durable Platinum Nanocatalyst for Proton Exchange Membrane Fuel Cells: Multiarmed Starlike Nanowire Single Crystal. *Angew. Chem. Int. Ed.* **50**, 422–426 (2011).
28. Liang, H. W. *et al.* A Free-Standing Pt-Nanowire Membrane as a Highly Stable Electrocatalyst for the Oxygen Reduction Reaction. *Adv. Mater.* **23**, 1467–1471 (2011).
29. Lee, E. P., Chen, J. Y., Yin, Y. D., Campbell, C. T. & Xia, Y. N. Pd-catalyzed growth of Pt nanoparticles or nanowires as dense coatings on polymeric and ceramic particulate supports. *Adv. Mater.* **18**, 3271–3274 (2006).
30. Lee, E. P. *et al.* Growing Pt nanowires as a densely packed array on metal gauze. *J. Am. Chem. Soc.* **129**, 10634–10635 (2007).
31. Formo, E., Lee, E., Campbell, D. & Xia, Y. N. Functionalization of electrospun TiO2 nanofibers with Pt nanoparticles and nanowires for catalytic applications. *Nano Lett.* **8**, 668–672 (2008).
32. Sun, S., Yang, D., Zhang, G., Sacher, E. & Dodelet, J. P. Synthesis and characterization of platinum nanowire-carbon nanotube heterostructures. *Chem. Mater.* **19**, 6376–6378 (2007).
33. Sun, S. H. *et al.* Template- and surfactant-free room temperature synthesis of self-assembled 3D pt nanoflowers from single-crystal nanowires. *Adv. Mater.* **20**, 571–574 (2008).
34. Sun, S. H., Jaouen, F. & Dodelet, J. P. Controlled Growth of Pt Nanowires on Carbon Nanospheres and Their Enhanced Performance as Electrocatalysts in PEM Fuel Cells. *Adv. Mater.* **20**, 3900–3904 (2008).
35. Sun, S. H. *et al.* Ultrathin single crystal Pt nanowires grown on N-doped carbon nanotubes. *Chem. Commun.* 7048–7050 (2009).
36. Yang, Z. *et al.* Sulfur-Doped Graphene as an Efficient Metal-free Cathode Catalyst for Oxygen Reduction. *Acs Nano* **6**, 205–211 (2012).
37. Ji, X. L. *et al.* Nanocrystalline intermetallics on mesoporous carbon for direct formic acid fuel cell anodes. *Nature Chem.* **2**, 286–293 (2010).
38. Hummers, W. S. & Offeman, R. E. Preparation of Graphitic Oxide. *J. Am. Chem. Soc.* **80**, 1339–1339 (1958).
39. Stamenkovic, V. R. *et al.* Improved oxygen reduction activity on Pt3Ni(111) via increased surface site availability. *Science* **315**, 493–497 (2007).
40. Service, R. F. Fuel Cells: Shrinking fuel cells promise power in your pocket. *Science* **296**, 1222–1224 (2002).
41. Hofstead-Duffy, A. M., Chen, D. J., Sun, S. G. & Tong, Y. Y. J. Origin of the current peak of negative scan in the cyclic voltammetry of methanol electro-oxidation on Pt-based electrocatalysts: a revisit to the current ratio criterion. *J. Mater. Chem.* **22**, 5205–5208 (2012).


## Acknowledgements

This work was funded by the Natural Sciences and Engineering Research Council of Canada (NSERC), the University of Waterloo and the Waterloo Institute for Nanotechnology.

## Author contributions

R.W. conducted the material preparations, characterizations and electrochemical tests. Z.C. supervised the project. All authors reviewed the manuscript.

## Additional information

**Supplementary information** accompanies this paper at http://www.nature.com/scientificreports

**Competing financial interests:** The authors declare no competing financial interests.

**How to cite this article:** Wang, R.Y. *et al*. Controlled Growth of Platinum Nanowire Arrays on Sulfur Doped Graphene as High Performance Electrocatalyst. *Sci. Rep.* **3**, 2431; DOI:10.1038/srep02431 (2013).